

# MODIFICATION OF THE INLET TO THE TERTIARY AIR DUCT IN THE CEMENT KILN INSTALLATION

Grzegorz Borsuk\*, Jacek Wydrych, Bolesław Dobrowolski

Opole University of Technology, Department of Thermal Engineering and Industrial Facilities,  
Mikołajczyka 5, 45-271 Opole, Poland

Rotary kiln installation forms a very complex system, as it consists of various components which affect cement production. However, some problems with particle settling are encountered during operation of tertiary air installation. This paper reports on the results of a study into gas-particle flow in a tertiary air duct installation. This flow was calculated using Euler method for air motion and Lagrange method for particle motion. The results in this paper demonstrate that study focus on the tertiary air installation is a practical measure without the analysis of other processes in the rotary kiln. A solution to this problem offers several alternatives of modifying the inlet to the tertiary air duct. As a result of numerical calculations, we demonstrate the influence of geometry of a rotary kiln modification on the number of large particles transported in the tertiary air duct. The results indicate that in order to reduce large particles, rotary kiln head geometry needs to be modified, and a particle settler should be installed at its outlet.

**Keywords:** pneumatic transport, CFD, particle concentration, tertiary air, rotary kiln

## 1. INTRODUCTION

In recent years, extensive work has been carried out with the aim of reducing energy consumption during cement production and gas emission reductions resulting from the use of alternative fuels from waste (Borsuk et al., 2016). Co-combustion of alternative fuels with coal in a rotary kiln is increasingly being considered as one of the environmentally friendly ways of disposing of waste. The development of new techniques of burning in kilns using the dry method with a multi-stage heat exchanger and a pre-decarbonization system related to the intensification of production and reduction of the sintering heat load (increase the life of the refractories), created the opportunity for greater use of alternative fuels. Because of the relatively low calorific value of alternative fuel and the required temperature difference between the combustion gases and the material in the sintering zone, the volume of fuel that can be burned in the main burner furnace is limited. The use of a larger proportion of these fuels will reduce the kiln efficiency and increase heat consumption. In contrast, significantly more alternative fuels, because of the lower temperature decarbonisation process may be used in the so-called decarbonisation pre-burner. The advantages of the initial decarbonisation technology and the possibility of adding waste fuel means that this solution is used in almost all kiln designs.

A part of the burner is equipped with typical type AS carbonizator (air separate) with the tertiary air. The rest of the burners operate as the AT type (air through), which involves carrying the combustion air through the kiln. Figure 1 is the illustration of the two systems of pre-decarbonization.

\*Corresponding author, e-mail: g.borsuk@po.opole.pl

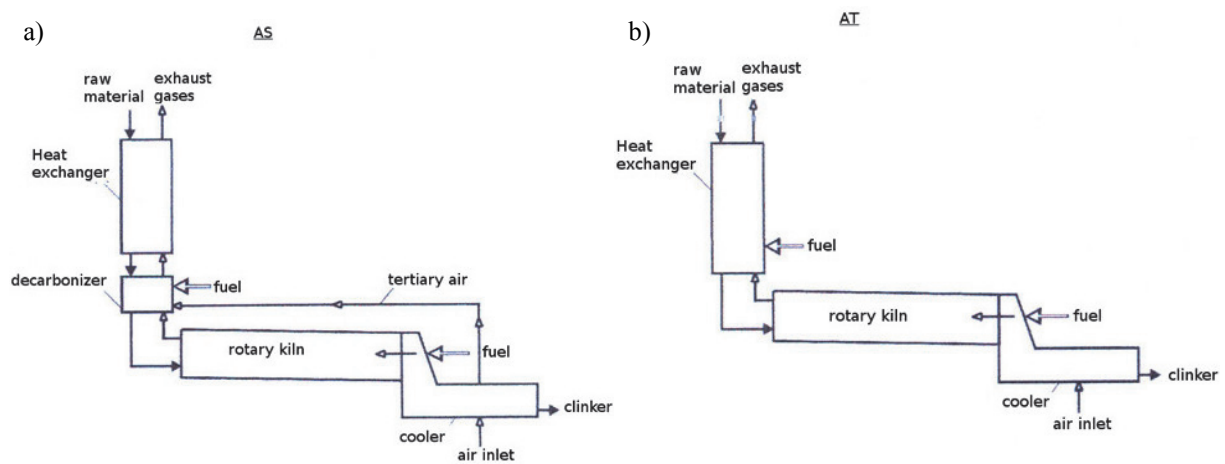


Fig. 1. Sketch of pre-carbonization systems in kiln during dry method of cement production;  
 a) air – separate, b) air – through

In the decarbonisation system, AS type alternative fuels can save up to 60% of heat in the burning process. However, in the AT system, fuel ratio is limited to 20%. AT system also does not involve initiation of the re-burning (multi-stage combustion), which is increasingly being used in decarbonizers to reduce NO<sub>x</sub> emissions.

Because these fuels are combusted outside of the kiln in the rising chamber, the process requires additional research into combustion conditions and the impact on gas emissions, especially NO<sub>x</sub> and CO. These problems are less important for the new kiln line with AS type pre-carbonisation systems, where the latest techniques in accordance with BAT are used. In the case of older system designs, it is necessary to run costly modernization works. Due to the limited possibility of performing tests on a working kiln, the use of alternative research approaches can get answers to interesting questions, without the drawbacks of losses in production and other operating risk, for example the influence of the air supply on burning process and decarbonisation. One of the approaches includes computer-aided modernization work, based on the use of Computational Fluid Dynamics (CFD). Despite their limited accuracy, simulation studies offer qualitative and quantitative analysis of very complex processes occurring in clinker production systems.

The subject of this paper is to report on a study involving optimization of the design of the installation for supply hot gases from the clinker cooler section to decarbonizer, where low-calorific fuel is burned. The principal problem is associated with the use of a relatively low pressure drop for the hot gas transport containing particles from clinker cooler. The presence of solid phase in the transported mixture causes great operational problems including the particle fall in the horizontal parts of the system and a change in flow direction. (Borsuk et al. 2014) presented preliminary results of numerical optimization of particle settler design, located just above the clinker cooler. The aim of this paper was to evaluate the impact of the design of a head on the separation efficiency of particles transported with the tertiary air.

Because of the clinker production process, a portion of the fuel can be burned in the preheater, and it is necessary to supply additional air (tertiary air), which should be extracted from the clinker cooler (Borsuk et al. 2014). The problem with tertiary air conveying is that clinker particles which are entrained from the cooler sometimes settle in the duct (Lain et al. 2012). However, for the purpose of optimization of operating conditions, it is necessary to understand processes which take place in the kiln. The specific requirements of the process include modification of a burner system to provide a burner design that can deliver efficient and reliable combustion. Yet, extensive use of this type of transport may bring about some problems that should be eliminated.

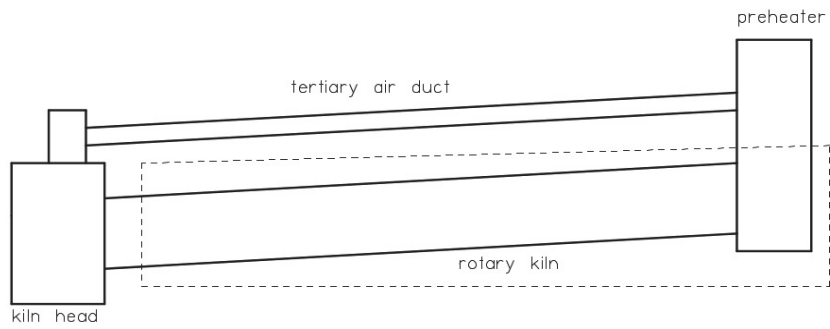


Fig. 2. General view of a rotary kiln

A numerical calculation domain was developed with the aim of describing the complex process of cement production. Due to this, only flow distribution through the kiln head was important for subsequent analysis. Consequently, the authors decided to consider a design of the cement kiln installation using only those elements which are necessary to bring correct results of pneumatic transport in the tertiary air duct. Figure 2 shows a general view of the rotary kiln system with the connection between the kiln head and the preheater. The section of the installation inside the dotted line was not considered in this analysis and, hence, there was a possibility to develop a calculation domain including tertiary air duct only. Figure 3 illustrates the rotary kiln head connected with the basic tertiary air duct.

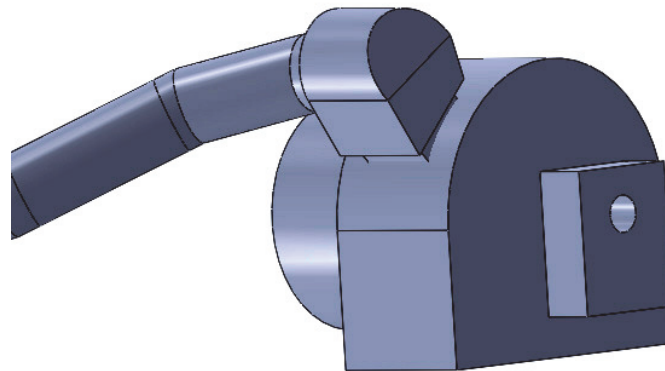


Fig. 3. Rotary kiln head for “basic” conditions – V0 design alternative

Flow parameters for the system are based on the following assumptions: constant velocity in the inlet cross-section depends on the gas flow rate to the kiln head, at the outlet of the kiln and constant pipeline pressure value was determined for the basic alternative for the appropriate distribution of gas stream in the kiln and tertiary air duct. Figure 4 shows the tertiary air duct with the inlet and outlet ports.

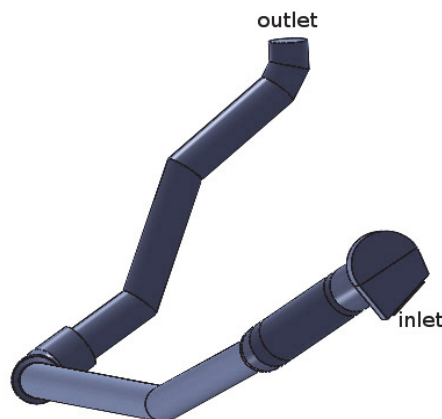


Fig. 4. Tertiary air duct

## 2. NUMERICAL MODELLING – PRINCIPLE OF OPERATION

In order to perform numerical calculations, a mathematical model consisting of equations of motion for the gaseous phase and coal dust particles was formulated. The air motion was described by the Euler method, and the particle motion – by the Lagrange method. To analyse the motion of the gas-particle polydisperse mixture, the PSI-Cell method was applied in this paper (Wydrych 2010).

Numerical calculations are based on the following assumptions: considered flow is isothermal, stationary and without phase changes, both phases are incompressible, gas motion is described in the uniform, generalized conservative form, isolating convection, diffusion and source components. As a consequence, we obtain:

$$\frac{\partial}{\partial x}(\rho U \phi) + \frac{\partial}{\partial y}(\rho U \phi) + \frac{\partial}{\partial z}(\rho U \phi) = \frac{\partial}{\partial x} \left( \Gamma_{\phi} \frac{\partial \phi}{\partial x} \right) + \frac{\partial}{\partial y} \left( \Gamma_{\phi} \frac{\partial \phi}{\partial y} \right) + \frac{\partial}{\partial z} \left( \Gamma_{\phi} \frac{\partial \phi}{\partial z} \right) + S_{\phi} + S_{\phi p} \quad (1)$$

where all the remaining components of the differential equations are presented in Table 1 (Borsuk et al. 2006).

Table 1. Elements of the formula (1)

Equation	$\phi$	$\Gamma_{\phi}$	$S_{\phi}$	$S_{\phi p}$
Continuity	1	0	0	0
Momentum equation in the $x_i$ axis	$u_i$	$\mu_{ef}$	$F_i - \frac{\partial p}{\partial x_i} + \frac{\partial}{\partial x_j} \left( \mu_{ef} \frac{\partial u_j}{\partial x_i} \right)$	$\overline{S_{u_i, p}}$

The coefficients  $\Gamma_{\phi}$  and  $S_{\phi}$  are dependent on the variable  $\phi$ . In the PSI-Cell method, it is assumed, that particles of the disintegrated phase are the sources of mass, momentum and energy occurring as additional components  $S_{\phi p}$  in equations of the continuous (gaseous) phase. The resulting system of equations is accompanied by suitable boundary and initial conditions. The above system of partial differential equations is non-linear. Particular equations are coupled, so they have to be solved with special numerical techniques.

The standard  $k$ - $\varepsilon$  model was used to calculate turbulence. The model transport equation for  $k$  is derived from the exact equation, while the model transport equation for  $\varepsilon$  was obtained using physical reasoning and bears little resemblance to its mathematically exact counterpart (Wang and Shirazi 2001).

In the derivation of the  $k$ - $\varepsilon$  model, it was assumed that the flow was fully turbulent, and the effects of molecular viscosity were negligible. The standard  $k$ - $\varepsilon$  model is, therefore, valid only for fully turbulent flows (Akili et al. 2001). The turbulence kinetic energy,  $k$  and its rate of dissipation  $\varepsilon$ , are calculated on the basis of the following transport equations (Kuan et al. 2007):

$$\frac{\partial}{\partial t}(\rho k) + \frac{\partial}{\partial x_i}(\rho k u_i) = \frac{\partial}{\partial x_j} \left[ \left( \mu + \frac{\mu_t}{\sigma_k} \right) \frac{\partial k}{\partial x_j} \right] + G_k + G_b - \rho \varepsilon - Y_M + S_k \quad (2)$$

$$\frac{\partial}{\partial t}(\rho \varepsilon) + \frac{\partial}{\partial x_i}(\rho \varepsilon u_i) = \frac{\partial}{\partial x_j} \left[ \left( \mu + \frac{\mu_t}{\sigma_{\varepsilon}} \right) \frac{\partial \varepsilon}{\partial x_j} \right] + C_{1\varepsilon} \frac{\varepsilon}{k} (G_k + C_{3\varepsilon} G_b) - C_{2\varepsilon} \rho \frac{\varepsilon^2}{k} + S_{\varepsilon} \quad (3)$$

where  $G_k$  represents the generation of turbulence kinetic energy due to the mean velocity gradients.  $G_b$  is the generation of turbulence kinetic energy due to buoyancy.  $Y_M$  represents the contribution of the fluctuating dilatation in compressible turbulence to the overall dissipation rate.  $C_{1\varepsilon}$ ,  $C_{2\varepsilon}$ , and  $C_{3\varepsilon}$  are

constants.  $\sigma_k$  and  $\sigma_\varepsilon$  are the turbulent Prandtl numbers for  $k$  and  $\varepsilon$ , respectively.  $S_k$  and  $S_\varepsilon$  are user-defined source terms. The turbulent (or eddy) viscosity  $\mu_t$  is computed by combining  $k$  and  $\varepsilon$  as follows:

$$\mu_t = \rho C_\mu \frac{k^2}{\varepsilon} \quad (4)$$

The model constants have the following default values:  $C_{1\varepsilon} = 1.44$ ,  $C_{2\varepsilon} = 1.92$ ,  $C_\mu = 0.09$ ,  $\sigma_k = 1.0$  and  $\sigma_\varepsilon = 1.3$ . In the calculations, spherical particles were assumed. The particle trajectory should be known during calculation of the source components of differential equations. The particle trajectory is calculated according to its equation of motion. If the phase density difference is considerable, the equation of particle motion can be written as (Levy and Mason 1998):

$$m_p \frac{du_p}{dt} = \frac{3}{4} C_D \frac{\rho m_p}{\rho_p d_k} |U - U_p| (U - U_p) + m_p g \quad (5)$$

and the aerodynamic drag coefficient given by

$$C_D = \begin{cases} \frac{24}{Re} \left( 1 + \frac{1}{6} Re^{2/3} \right) & Re \leq 1000 \\ 0.424 & Re > 1000 \end{cases} \quad (6)$$

### 3. DETERMINATION OF BOUNDARY CONDITIONS FOR FURTHER CALCULATION

The input regarding gas flow rate incoming to the rotary kiln head was obtained from the cement factory monitoring system. Taking into account the area of the inlet cross-section the velocity was set at 5.538 m/s. The pressure drop between the inlet to head and the outlet from tertiary air pipe was used as the input for the calculations of mixture flow distribution. The primary step was to calculate the pressure at the outlet to the kiln, as the flow distribution is the same at the start of the analysis. Over 70% of the flow rate value at the inlet to the head is transported through the kiln. A minor proportion is transported through the tertiary air installation.

Figure 5 presents a velocity profile for the basic conditions. In the tertiary air duct velocity is contained in the range from 0 to 20 m/s. Figure 6 presents the particle concentration in selected cross sections of the kiln head.

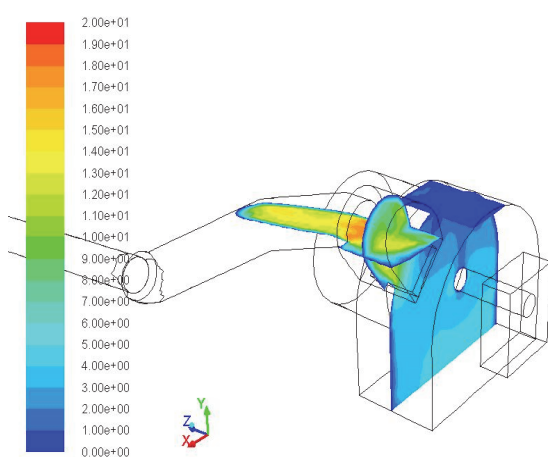


Fig. 5. Velocity profile [m/s] in V0 alternative

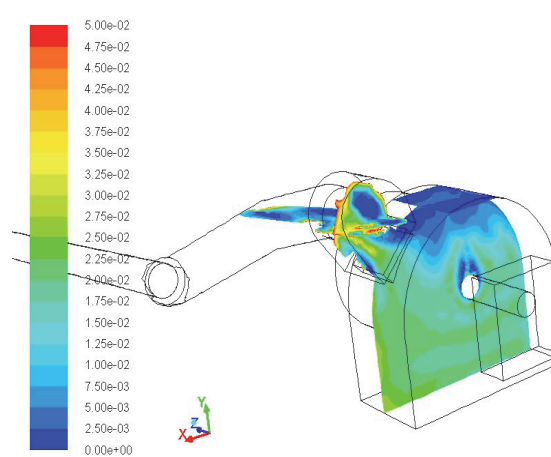


Fig. 6. Particle concentration [kg/m<sup>3</sup>] in V0 alternative

For the particle calculation, Rosin-Rammler-Sperling distribution was used and 10 fractions of particles with the range from 15 to 600  $\mu\text{m}$  were determined.

Table 2. Particle ratios

$d$ [ $\mu\text{m}$ ]	Percentage
15	7.51
35	9.39
55	10.32
75	14.12
110	17.16
150	18.66
220	16.67
350	5.15
450	0.95
600	0.07

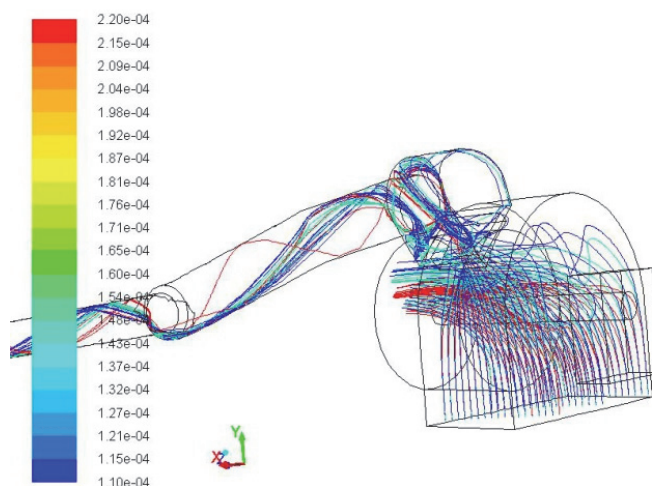


Fig. 7. Particle trajectories ( $d_{110}$ ,  $d_{150}$ ,  $d_{220}$   $\mu\text{m}$ ) – V0 alternative

Table 2 presents the distribution of particles in each fraction determined as a part of the total mass flow rate. The same number of intake points for all particle fractions was assumed in the calculations. The adopted boundary conditions gave the expected calculations of the pressure drop values. Calculations were performed using ANSYS Package (Ansys Inc 2015). Figure 7 presents particle trajectories in the head of rotary kiln.

#### 4. TERTIARY AIR INSTALLATION WITH SOLID PARTICLE SETTLER

##### *4.1. Installation of auxiliary settler at the end of the kiln head*

A special settler located just after the outlet of the kiln head as one of the tertiary air installation sections was used for the basic conditions obtained from the initial calculations (for the V0 alternative). Selected alternatives of the modified design are shown in Fig. 8.

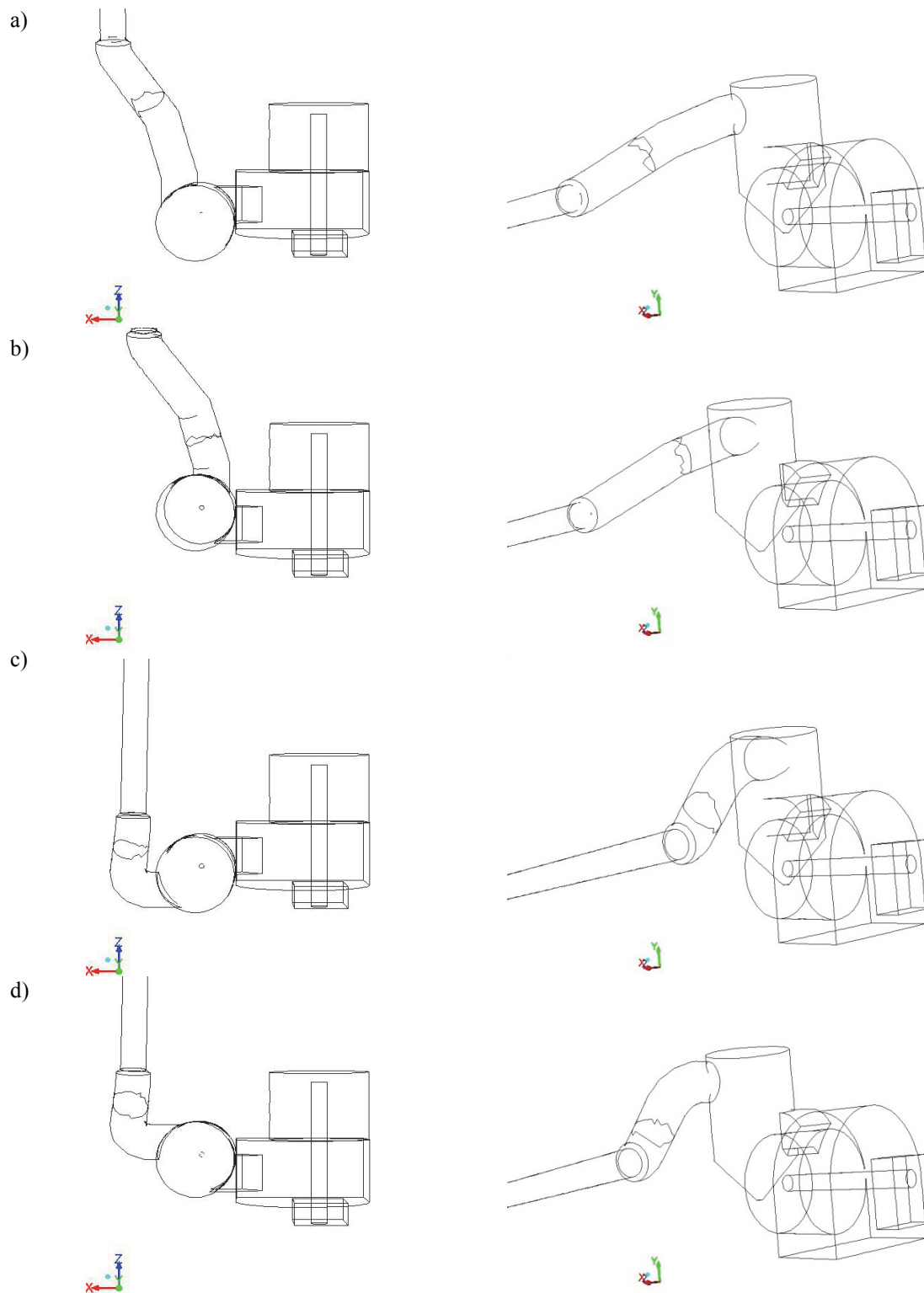


Fig. 8. Considered modifications of the settler for;  
 a) V1 alternative, b) V2 alternative, c) V3 alternative, d) V4 alternative

In V1 and V2 alternative designs, the inlet and the outlet in the settler are inclined at  $90^\circ$  angle, whereas in V3 and V4 alternatives, they are located along the same axis but at another angle relative to the circular base of the settler. In V1 and V3 alternatives, the settler is situated further from the rotary kiln, whereas in V2 and V4 alternatives – closer to the kiln. In each of the considered alternatives, some particles are transported with the gas through the tertiary air duct, and a “rope” of particles is noticeable particularly in V2 alternative. For this set, the largest number of particles is transported through the tertiary air duct, so the working conditions are the least beneficial of all possible.

#### 4.2. Modification of the rotary kiln head

The design of the rotary kiln head was the same in the previously considered alternatives. In this section, we consider modifications to the geometry of this head. This time, we redesigned kiln head so as to increase the volume of the head. Figure 9a shows alternative design 5 with a modified head. The settler located just after the outlet to the tertiary air installation was used in the new design of the rotary kiln head, Figs. 9b - 9c illustrate the selected alternatives. In another alternative design, V6, the settler is situated in front to the head, whereas in V7 alternative it is found in the back.

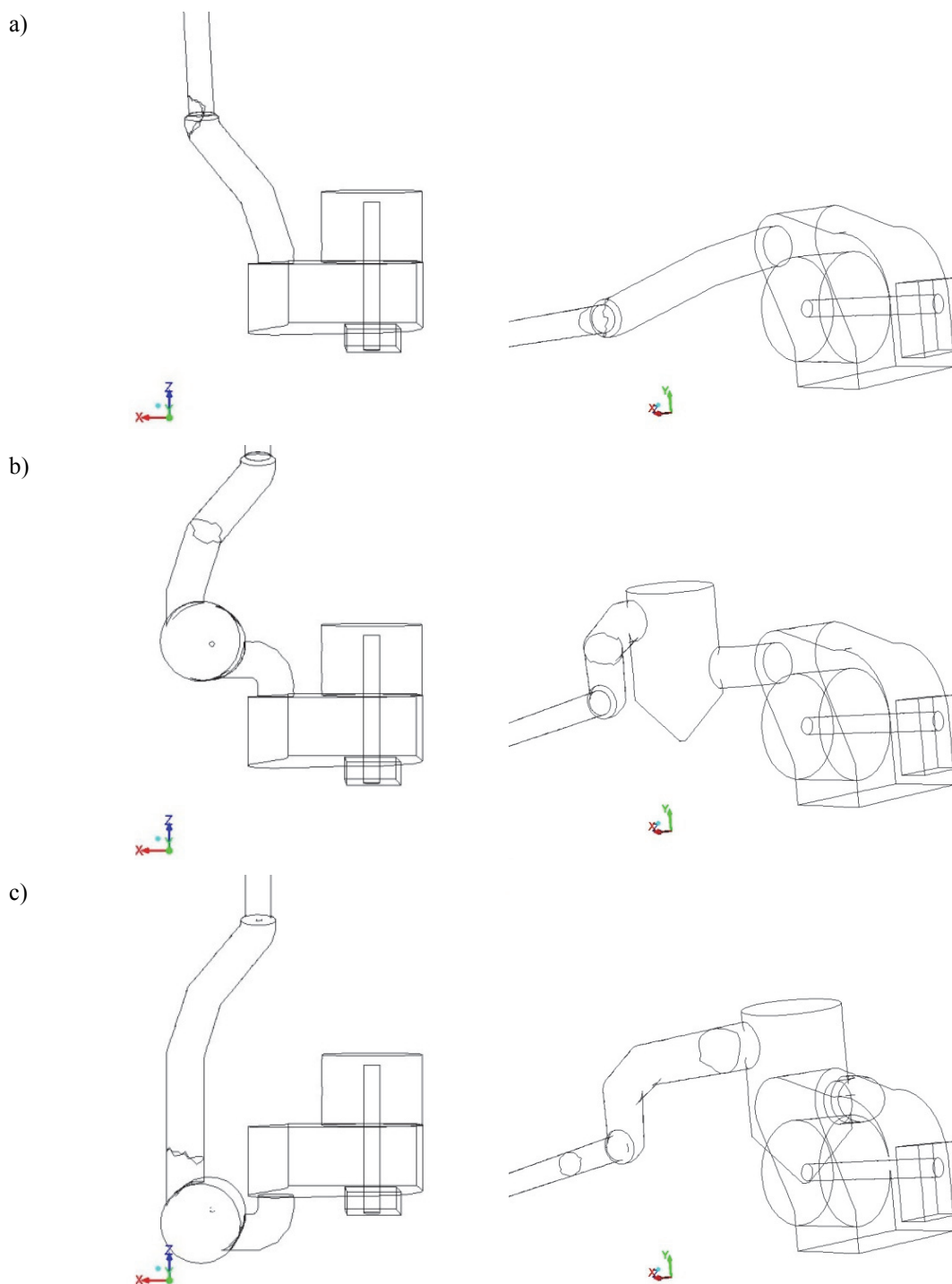


Fig. 9. Considered modifications of the rotary kiln head;  
a) V5 alternative, with settler; b) V6 alternative, c) V7 alternative

### 5. PARTICLE CONVEYING

The next step of the study involved counting particles transported in the tertiary air installation. The data in Fig. 10 indicate the number of particles at the outlet from tertiary air installation for “basic” conditions and the subsequent six alternatives for particle diameters in the range 110 - 350  $\mu\text{m}$ , and in Fig. 11 one can find numbers of particles diameters within the range of 15 - 75  $\mu\text{m}$ , respectively.

Figure 10 shows that the best results in terms of reducing the number of large particles transported in the tertiary air installation without modification of the rotary kiln head are obtained in the V1 alternative design, where the inlet and outlet are positioned relative to the settler at an angle of 90°. For smaller diameters, the greatest reduction of the particle number was found in V3 alternative (Fig. 11).

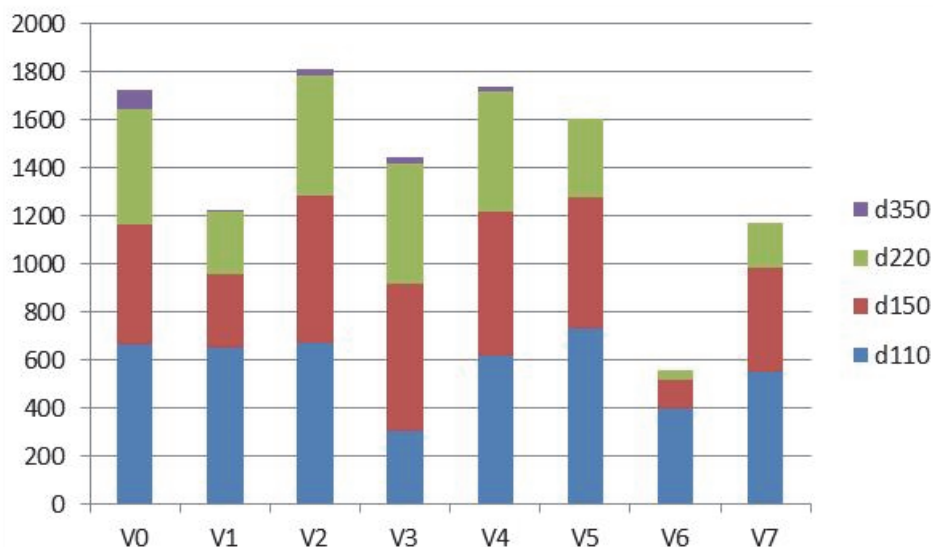


Fig. 10. Number of particles at the outflow from tertiary air installation within the 110-350  $\mu\text{m}$  range of diameters

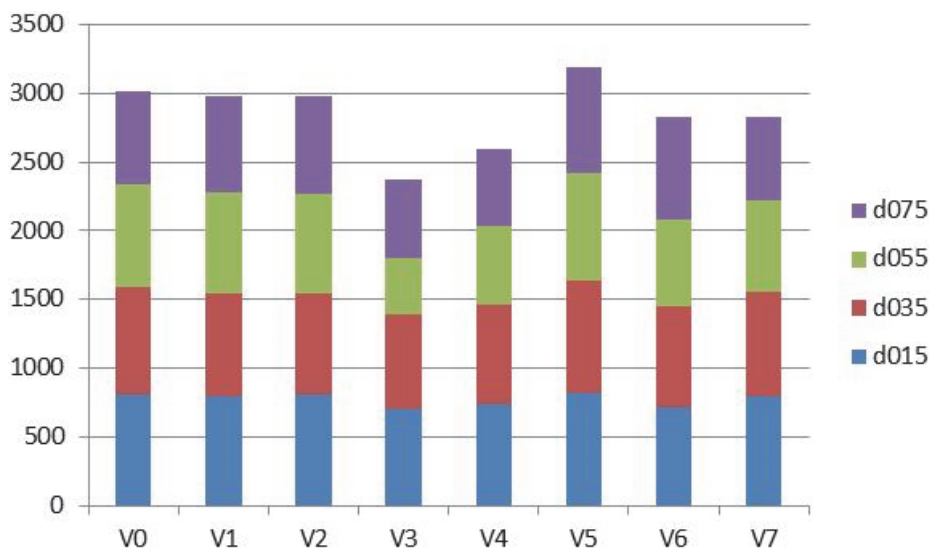


Fig. 11. Number of particles at the outflow from tertiary air installation within the 15-75  $\mu\text{m}$  range of diameters

After modifications to the geometry of the rotary kiln head, the number of particles transported in the tertiary air duct remains at almost the same level (V5). This modification of the head resulted in a reduction of large particles in the tertiary air installation. The combination of the modified kiln head geometry and particle settler in the front leads to a reduction of the number of particles in a larger diameters range (V6).

To gain a better insight into the outcome of the study, the next step involved the calculation of the particle mass flow rate for each of the considered alternatives. Figure 12 shows the results of the calculation.

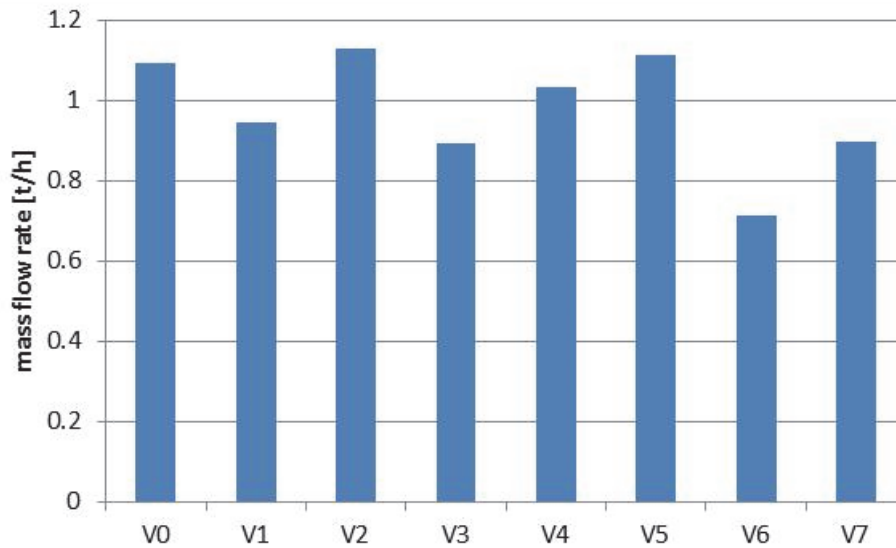


Fig. 12. Mass flow rate for all variants considered

In the V3 and V4 alternatives considered above, the mass flow rate is smaller than the basic system, but the ratio of particles with the diameter exceeding 150  $\mu\text{m}$  is greater. This is probably related to the outcome of the formation of a „rope” of particles passing through the settler. This phenomenon is even more visible in V2 alternative, where most particles exit from the head after a distribution in the pipeline avoiding the middle part of the settler.

## 6. CONCLUSIONS

We consider a tertiary air installation design with a focus on a solution including only its part. In this study the analysis of other processes in the rotary kiln is omitted. We only consider pressure drop as a boundary condition for gas-particle mixture flow through the tertiary air duct. From the results of numerical calculations based on the above simplifications the following conclusions can be drawn:

- The use of a dedicated settler upstream in tertiary air duct leads to a decrease in the number of particles transported with the gas. This, however, is relative to the geometry of the settler.
- The modification of the rotary kiln head geometry described in this paper affects the number of large particles transported in the tertiary air duct.
- For achieving the greatest reduction in the number of particles it is necessary to modify the geometry of the rotary kiln head and apply a particle settler in the front of the head.

## SYMBOLS

$C_D$	aerodynamic drag coefficient
$C_{1\varepsilon}, C_{2\varepsilon}, C_{3\varepsilon}$	constants
$G_k$	generation of turbulence kinetic energy due to the mean velocity gradients
$G_b$	generation of turbulence kinetic energy due to buoyancy
$m_p$	mass of the particle

$S_k, S_\varepsilon$	user-defined source terms
$S_\phi$	source term
$Y_M$	contribution of the fluctuating dilatation in compressible turbulence to the overall dissipation rate

#### Greek symbols

$\phi$	generalized dependent variable
$\Gamma_\phi$	coefficient of diffusion transport
$\sigma_k$	turbulent Prandtl numbers for $k$
$\sigma_\varepsilon$	turbulent Prandtl numbers for $\varepsilon$

#### REFERENCES

- Akili H., Levy E.K., Sahin B., 2001. Gas-solid flow behavior in a horizontal pipe after a 90° vertical-to-horizontal elbow. *Powder Technol.*, 116, 43-52. DOI: 10.1016/S0032-5910(00)00360-0.
- ANSYS Fluent, Release 15.0, ANSYS Inc.
- Borsuk G., Dobrowolski B., Nowosielski G., Wydrych J., Duda J., 2016. Numerical simulation of thermal-hydraulic processes in the riser chamber of installation for clinker production. *Arch. Thermodyn.*, 37, 127-142. DOI: 10.1515/aoter-2016-0009.
- Borsuk G., Dobrowolski B., Wydrych J., 2006. Gas - solids mixture flow through a two - bend system. *Chem. Process Eng.*, 27, (3/1), 645-656.
- Borsuk G., Wydrych J., Dobrowolski B., 2014. Optimization of particle settler in tertiary air duct in the cement kiln installation, In: *Aktualne Zagadnienia Energetyki*, Politechnika Wroclawska, 115-124.
- Fidaros D.K., Baxevanou C.A., Dritselis C.D., Vlachos N.S., 2007. Numerical modelling of flow and transport processes in a calciner for cement production. *Powder Technol.*, 171, 81-95. DOI: 10.1016/j.powtec.2006.09.01.
- Hu Z., Lu J., Huang L., Wang S., 2006. Numerical simulation study on gas-solid two-phase flow in pre-calciner. *Commun. Nonlinear Sci. Numer. Simul.*, 11, 440-451. DOI: 10.1016/j.cnsns.2004.07.004.
- Kuan B., Yang W., Schwarz P., 2007. Dilute gas-solid two-phase flows in a curved 90° duct bend: CFD simulation with experimental validation. *Chem. Eng. Sci.*, 62, 2068-2088. DOI: 10.1016/j.ces.2006.12.054.
- Lain S., Sommerfeld M., 2012. Numerical calculation of pneumatic conveying in horizontal channels and pipes: Detailed analysis of conveying behaviour. *Int. J. Multiphase Flow*, 39, 105-120. DOI: 10.1016/j.ijmultiphaseflow.2011.09.006.
- Lederer H., 1996. A new rotary kiln burner technology. *World cement*, 27 (12), 45-48.
- Levy A., Mason D.J., 1998. The effect of a band on the particle cross-section concentration and segregation in pneumatic conveying systems. *Powder Technol.*, 98, 95-103. DOI: 10.1016/S0032-5910(97)03385-8.
- Saidura R., Hossaina M.S., Islama M.R., Fayazb H., Mohammed H.A., 2011. A review on kiln system modelling. *Renewable Sustainable Energy Rev.*, 15, 2487-2500. DOI: 10.1016/j.rser.2011.01.020.
- Wang J., Shirazi S.A., 2001. A CFD based correlation for mass transfer coefficient in elbows. *Int. J. Heat Mass Transfer*, 44, 1817-1822. DOI: 10.1016/S0017-9310(00)00222-2.
- Wydrych J., 2010. Comparative analysis of the methods of simulation of flow in boiler dust systems. *Chem. Process Eng.*, 31 (4), 603-656.
- Zhou Z., Zhu H., Wright B., Yu A., Zulli P., 2011. Gas-solid flow in an ironmaking blast furnace-II: Discrete particle simulation. *Powder Technol.*, 208, 72-85. DOI: 10.1016/j.powtec.2010.12.005.

Received 16 June 2015

Received in revised form 01 August 2016

Accepted 05 October 2016